

Numerical Modeling and Simulation of Melting Phenomena for Freeze Valve Analysis in Molten Salt Reactors

Davide Tartaglia, Antonio Cammi, Carolina Introini & Stefano Lorenzi

To cite this article: Davide Tartaglia, Antonio Cammi, Carolina Introini & Stefano Lorenzi (2023) Numerical Modeling and Simulation of Melting Phenomena for Freeze Valve Analysis in Molten Salt Reactors, Nuclear Science and Engineering, 197:12, 3058-3081, DOI: [10.1080/00295639.2023.2229576](https://doi.org/10.1080/00295639.2023.2229576)

To link to this article: <https://doi.org/10.1080/00295639.2023.2229576>



© 2023 The Author(s). Published with license by Taylor & Francis Group, LLC.



Published online: 08 Aug 2023.



Submit your article to this journal [↗](#)



Article views: 455



View related articles [↗](#)



View Crossmark data [↗](#)



Numerical Modeling and Simulation of Melting Phenomena for Freeze Valve Analysis in Molten Salt Reactors

Davide Tartaglia, Antonio Cammi, Carolina Introini, and Stefano Lorenzi^{ID*}

Politecnico di Milano, Department of Energy, via La Masa 34, Milano, Italy

Received January 31, 2023

Accepted for Publication June 8, 2023

Abstract — *In recent years, molten salt reactors (MSRs) have gained new momentum thanks to their potential for innovation in the nuclear industry, and several studies on their compliance with all the expected safety features are currently underway. In terms of passive safety, a strategy currently envisaged in accidental scenarios is to drain by gravity the molten salt, which acts both as fuel and coolant, in an emergency draining tank, ensuring both a subcritical geometry and proper cooling. To activate the draining system, a freeze plug, made of the same salt used in the core, is expected to open when the temperature in the core reaches high values. Up to this point, the freeze valve is still a key concept in the molten salt fast reactor (MSFR), and special attention must be paid to its analysis, given the requirement for passive safety, especially focusing on melting and solidification phenomena related to the molten salt mixture.*

This work aims to contribute to the macroscale modeling of melting and solidification phenomena relevant to the analysis of the freeze valve behavior. In particular, the focus is on the identification of the numerical models that can be adopted to achieve the quantitative insights needed for the design of the freeze valve. Among the ones available in the literature, the most appropriate models were selected based on a compromise between accuracy and computational efficiency. A critical look at the models allows for a synthetic and consistent formulation of the numerical models and their implementation in the open-source software OpenFOAM. The code was subsequently verified using analytical and numerical solutions already well established in the literature.

A good agreement between the results produced by the developed solver and the reference solutions was obtained. In the end, the code was applied to simple case studies related to the freeze valve system, focusing on recognizing whether the developed code can model physical phenomena that can occur in a freeze valve. The results of the simulations are encouraging and show that the code can be used to model single-region melting or solidification problems. As such, this work constitutes a starting point for further development of the code, intending to achieve better quantitative predictions for the design of a freeze valve.

Keywords — *Molten salt fast reactor, passive safety, melting and solidification, numerical methods.*

Note — *Some figures may be in color only in the electronic version.*

*E-mail: stefano.lorenzi@polimi.it

This is an Open Access article distributed under the terms of the Creative Commons Attribution-NonCommercial-NoDerivatives License (<http://creativecommons.org/licenses/by-nc-nd/4.0/>), which permits non-commercial re-use, distribution, and reproduction in any medium, provided the original work is properly cited, and is not altered, transformed, or built upon in any way. The terms on which this article has been published allow the posting of the Accepted Manuscript in a repository by the author(s) or with their consent.

I. INTRODUCTION

Generation-IV reactors^[1] are nuclear reactor concepts having the potential to bring various benefits to the nuclear industry, including increased safety, reduced proliferation risks, economical affordability, sustainability of the fuel cycle, and management of the waste inventory. Among them, the molten salt fast reactor (MSFR) is the

current reference design studied within the Generation-IV International Forum, and its safety barriers are the object of the SAMOSAFER European project.^a A mixture of chloride or fluoride salt containing the dissolved nuclear fuel is pumped and circulated through the primary system, acting as coolant and fuel.^[2] In case of an accident, the molten salt is drained by gravity from the core to a casing located below the core, where proper cooling and subcriticality are ensured. The draining system is connected through 16 pipes to the bottom of each one of the external loops.

To enhance the passive safety feature of the reactor, the MSFR design is provided with freeze valves. Such a component was first used in the Molten Salt Reactor Experiment (MSRE) as a way to overcome the difficulty of finding a reliable mechanical valve that could bear the aggressive environment of the system.^[3] The freeze valve allows for draining of the molten salt when an accident makes the temperature of the core rise over acceptable levels. In this case, the valve melted by the heat stored in metal plates in contact with it, kept hot by electric resistances. However, as designed in the MSRE, the freeze valve was not a fully passive safety feature.^[3] For this reason, novel commitment is necessary to achieve a design that is compliant with the requirement for passive safety. The modern concept of a MSFR envisions the use of a freeze valve as well, positioned vertically in a portion of the draining piping in the proximity of the core. The freeze valve is still considered today as a valuable solution to be implemented in future molten salt reactors (MSRs), not only because of the compatibility of the material in the demanding environment of the core. Especially after the Fukushima Daiichi accident, the concept of passive safety is a fundamental requirement for nuclear reactors, and the ability of the valve to self-modulate its state, using the phase change, in response to temperature variations in the core has frequently been equated to safety function passivity. For this reason, it is fundamental to be able to reach a fully passive design of the freeze valve, and the capability of the valve to open in any accidental scenario, including a loss of outside power, is of great importance.

Melting and solidification of the fuel salt play a key role in the design and safety of the MSFR, such as the design of the freeze plug,^[4] the analysis of accident scenarios where the solidification of the salt might be a risk,^[5] or the possible formation of a frozen salt film on the reactor vessel walls, protecting them from

corrosion.^[6] A mathematical description of the melting and solidification problem allows for a quantitative description of a phase-change transient. The most basic mathematical description of melting and solidification phenomena is due to Josef Stefan,^[7] and the respective mathematical problem is known as the Classical Stefan Problem. However, this problem does not have exact or approximate analytical solutions for many real engineering situations. For instance, most practical situations are multidimensional in nature, while analytical solutions are only available in one dimension.^[8] For this reason, the urge for the development of numerical methods has been present in the scientific literature since at least the late 1980s.

However, the numerical modeling of the phase change is a challenging task due to two main issues. On the one hand, the phase change from liquid to solid is a multiscale process, meaning that the dynamics of the phase change are governed by different physical phenomena that span from the atomic scale to the macroscale.^[9] The coupling of these phenomena represents a challenge both to the physical modeling and to the discretization process of the numerical models. On the other hand, with the macroscale approach, two other challenges emerge: (1) the choice of the appropriate values for the thermo-physical properties of the solid phase that are required to embed all the complexity of a possibly anisotropic microstructure (as in the case of the eutectic solidification of the FLiNaK) in averaged quantities, such as the thermal conductivity tensor, the equivalent elastic-plastic modulus, the equivalent thermal stress tensor, and possibly others^[10]; and (2) the nonlinearity of the macroscale formulation, as the liquid front depends on the temperature of the system, and vice versa.

Historically, the study of phase-change materials (PCMs) has been a big incentive for the development of numerical methods for melting and solidification. Nowadays, the study of PCM using computational fluid dynamics is widespread and has been documented in several papers. (Reference [11] provides a review on the topic.) Typically, there are two main groups of numerical phase-change models: fixed-grid (or physical-grid) and variable-grid (or transformed-grid) models. In the latter, two sets of equations are implemented, one for each phase (solid and liquid). Indeed, the grid is adapted to the interface location, and the two separate domains are coupled using transference terms between the phases.

On the other hand, fixed-grid methods consider a single set of discretized conservation equations, valid both for the solid and the liquid domains. Differently from variable-grid methods, the interface is not tracked

^a See <https://samosafer.eu/>.

explicitly, but is it reconstructed a posteriori after an appropriate field variable. Hence, no run-time modification of the computational domain is required. The energy conservation and the Navier-Stokes equations are modified to properly take into account the two main phenomena that take place during phase change, namely, latent heat and velocity transition, the latter being the momentum exchange between the solid and the liquid phases. The main advantage of the fixed-grid methods is their simplicity, which has determined their rise in popularity, making them a standard approach in the field of the numerical modeling of metallurgical solidification processes and PCMs.^[11]

Since in such methods the discontinuity is not treated by separating the computational domain, the interface is “smeared” in a finite length, often called a “mushy zone.” Such a halfway state is determined by the presence of both solid and liquid in different proportions, according to the temperature of the mixture. Indeed, excluding two exceptions, namely, eutectic systems and pure elements, in most solidification systems the phase change from liquid to solid and the relative evolution of latent heat will occur over a temperature range in which both the liquid and solid coexist.^[12] For this reason, the fixed-grid methods are conceptually more suitable for nonisothermal phase changes. However, they have been largely adapted for use also for isothermal phase changes, even if in this case the interface between solid and liquid is sharp, by forcing the mushy region to be as localized as possible.

A few preliminary numerical analyses of the freeze plugs already exist, such as in Refs. [4,13–15], and they all make use of fixed-grid numerical methods for the phase change to make quantitative predictions about the melting times and other significant engineering quantities of the valves. In Ref. [13], a high-temperature molten salt test loop was constructed and tested, both numerically and experimentally. The working fluid was FLiNaK salt, while the valve was made of Hastelloy C276 and set into a horizontal position, having the shape of a pipe squashed in the middle portion. The numerical analysis consisted of a steady-state analysis of the thermal behavior, using a Finite Elements (FE) calculation, which was validated by the experimental setup.

In Ref. [14], a freeze valve was built and experimentally studied to investigate which phenomena impacted the melting time of the freeze valve. The study allowed for assessing the fundamental parameters to be considered in the construction of a freeze valve, such as the liquid temperature, the depth, the diameter, and the thermal diffusivity. In Ref. [4], a numerical study was conducted to offer preliminary insights into different engineering solutions and parameters. The salt considered in this case was LiF₄,

and two possible configurations were investigated: the first was called “single plug,” which was a single cylinder of solid salt, and the other was called “multiple plugs,” in which several cylinders of salt were inserted in a drilled metal plate. In Ref. [15], taking advantage of the knowledge given by experiments and using numerical simulations, useful recommendations and guidelines for the design of a cold plug were provided.

In Ref. [10], a multiscale model for the SWATH-S (an experiment dealing with the solidification of FLiNaK salt) was developed with the aim of taking into account the coupling between the phenomena occurring at the macroscale with those that take place at the mesoscale. The macroscale model was developed using an arbitrary Lagrangian-Eulerian method, where the solid is described by a Lagrangian approach and the liquid by an Eulerian approach. Furthermore, the mesh was adapted to the shrinkage of the solid phase, and a novel thermodynamically consistent derivation of the conservation equations was developed. For what concerns the mesoscale model, it is refined enough to describe the phase segregation in the solid phase thanks to a thermodynamical model conceptually similar to the macroscale one.

If on one hand, models like the latter are precious to estimate the parameters for the macroscale models, they are hardly scalable to large systems due to the intensive computational effort required. The aim of this work is to provide a previously developed OpenFOAM solver for MSFR analysis^[16–19] with the capability to model the freeze plug in operational- and safety-related transients. Due to the requirement of modeling the entire MSFR system, the development focus is on the fixed-grid approach with a macroscale phase-change representation [e.g., apparent Heat Capacity (AHC) method^[20] and Source Term (ST) method].^[21] This way, the solver does not need Lagrangian mesh capabilities and does not depend on complex thermodynamics mesoscale models that can hinder the simulation of a full-scale system.

This paper is organized as follows. A review of the numerical modeling used in the developed code is formalized in Sec. II. Afterward, the code is verified in simple benchmark test cases (Sec. III). Finally, the verified code is used to simulate freeze valve-like scenarios to test and see which phenomena the code can model when dealing with realistic cases (Sec. IV).

II. THEORETICAL FRAMEWORK AND NUMERICAL MODELING

As mentioned previously, the two main physical phenomena that have to be addressed in the numerical

modeling for melting and solidification are the latent heat and the velocity transition. From a theoretical perspective, the present work adopts the framework of the Continuum Mixture Theory (CMT)^[22] in which each phase constituting the mixture is seen as an individual subsystem, given that the interaction terms with other phases are properly treated, and assuming that the properties of the mixture can be described as mathematical consequences of properties of the constituting phases and that the mean collective mixture behavior is governed by equations similar to those governing the individual component (single-fluid model).

In this framework, a few simplifying assumptions allow for writing the equations for the mass, momentum, and energy conservation in a familiar form, suitable to be solved by the established numerical procedure for coupled elliptic partial differential equations with slight modifications for the specificity of the melting problem. Assumptions invoked in the development of such equations include (1) saturated mixture conditions, (2) laminar, constant viscosity, and Newtonian flow in the liquid phase, (3) thermophysical properties independent from pressure and temperature, meaning constant-phase specific heat capacities ($c_{p,l}$ and $c_{p,s}$), and constant-phase densities (ρ_l and ρ_s), except for variations in the buoyancy term for the liquid, (4) validity of the Boussinesq approximation, and (5) local thermodynamic equilibrium. In addition, (6) the solid phase is assumed to be nondeforming and free of internal stress, while (7) the multiphase region is viewed as a porous solid characterized by an isotropic permeability.^[22] Moreover, in the present work, (8) the salt is seen as a pure substance, without any subconstituent. This is done for the sake of simplicity, since the objective of the present work is to address the numerical models for the solution of the melting problem. Nonetheless, the CMT allows for taking into account the transport of constituents in a natural way, as can be seen in the pioneering work of Bennon and Incropera.^[22]

However, some of these simplifying assumptions might introduce errors for melting and solidification problems, i.e., assumptions (3), (4), and (5) are acceptable if the solid and the liquid are within a small temperature range from the melting temperature, but they can generate large errors when larger temperature variations are considered. The impact of higher-order terms on the dependency of the density from the temperature for the FLiNaK salt has been extensively studied in Ref. [10]. Here it is demonstrated that, while it is true that the impact of the solute-driven convection is important close to the interface, its relevance is limited in the very proximity of the interface. When moving away from the interface, these

gradients are rapidly smeared out. On the contrary, the thermal gradients can extend over the whole domain. Hence, the effective influence of solute buoyancy in the velocity field generated in the domain is usually much smaller than that of thermal buoyancy.

To achieve higher accuracy in this aspect of the modeling, future work could include solute-driven convection terms and the second-order terms evaluated in Ref. [10]. Moreover, while assumption (6) is useful in the scope of this work to focus on the numerical modeling of the melting phenomena, a complete analysis of the freeze valve should likely include the modeling of internal stresses in the solid. For instance, Ref. [10] shows that thermal gradients produce thermal stresses close to the interface. Other clusters of thermal stresses might be present close to the walls due to the constraint of the boundary and to the heat flux coming from the cooling system of the valve. Moreover, during melting transients, the thermal stresses produced by the high thermal gradient might induce cracks in the solid. Assumption (7) is largely used in studies of phase-change processes,^[11] and it is modeled by a Darcy source term (DST) in the momentum equation. In the case of the FLiNaK salt, the coefficient of this source term can be calculated by mesoscale models, as in Ref. [10]. With these assumptions, the conservation equations of the system are

$$\frac{\partial(\rho\vec{u})}{\partial t} + \nabla \cdot (\rho\vec{u}) = 0 \quad , \quad (1)$$

$$\frac{\partial(\rho\vec{u})}{\partial t} + \nabla \cdot (\rho\vec{u} \otimes \vec{u}) = -\nabla p + \nabla \cdot \left(\frac{\rho}{\rho_l} v_l \nabla \vec{u} \right) + \rho \vec{g} + \vec{F} \quad , \quad (2)$$

$$\frac{\partial(\rho h)}{\partial t} + \nabla \cdot (\rho h \vec{u}) = \nabla \cdot (k \nabla T) + Q \quad , \quad (3)$$

where

\vec{u} = mixture velocity

T = mixture temperature

p = mixture pressure

ρ = mixture density

h = mixture-specific enthalpy

k = mixture thermal conductivity

ρ_l = density of the liquid phase
 ν_l = viscosity of the liquid phase.

The \vec{F} term present in Eq. (2) models the exchange terms between the solid and liquid, and the choice of its physical and numerical modeling is called velocity transition modeling (VTM). The momentum source term \vec{F} depends on the volume liquid fraction g (not to be confused with the gravity force \vec{g}), and the liquid fraction depends on the temperature, so that the momentum and the energy equations are coupled. Q is any heat source that may be added according to the specific case.

In the energy equation, the specific enthalpy h depends on the temperature T , and a closure relation must be defined to close the system. Together with the choice of the closure equation, the numerical modeling of the energy equation is called latent heat modeling (LHM).

II.A. Latent Heat Modeling

Analytically, latent heat is modeled through the Stefan condition,^[8] which states that the latent heat released due to the interface displacement equals the net amount of heat delivered to or from the interface itself per unit area per unit time:

$$\rho L v = [\vec{q} \cdot \vec{n}]_{solid}^{liquid} , \quad (4)$$

where L is the specific latent heat, v is the velocity of the interface, \vec{q} is the heat flux, and \vec{n} is the normal to the interface.

However, this condition does not represent how fixed-grid methods deal with LHM because they do not track explicitly the position of the interface, but the condition must be imposed implicitly directly in the energy equation. In fact, in the framework of CMT, we can define average thermodynamic quantities on a certain volume so that the presence of each phase can be deduced from the mean quantities, such as the mean volumetric enthalpy H .^[21] The most relevant definitions used in this work are

$$\rho = g\rho_l + (1 - g)\rho_s , \quad (5)$$

$$h = fh_l + (1 - f)h_s , \quad (6)$$

$$h_s = \int_{T_m}^T c_{p,s} dT' + h_0 , \quad (7)$$

$$h_l = \int_{T_m}^T c_{p,l} dT' + L + h_0 , \quad (8)$$

where

ρ = density

h = specific enthalpy of the mixture

g = volume liquid fraction

f = mass liquid fraction

h_0 = a constant offset value, which can be seen as the specific enthalpy of the solid at the melting temperature T_m .

The thermophysical properties are considered independent from the temperature and different from solid to liquid, i.e., $c_{p,l} \neq c_{p,s}$ and $\rho_l \neq \rho_s$. This is not a common choice in literature; usually, the thermophysical properties, especially density, are taken to be equal from solid to liquid (as in Refs. [11,21,23–25], including the built-in option proposed in OpenFOAM^[26]). CMT on the other hand allows for naturally taking into account different thermophysical properties, which can allow for greater accuracy in the simulations, being a model closer to the physical reality. The vast majority of real substances do not have constant thermophysical properties across the phase transition. Assuming $c_{p,l}$ and $c_{p,s}$ independent from the temperature in a range close to the melting temperature, the average specific enthalpy h can be written as

$$h_s = c_{p,s}(T - T_m) + h_0 ,$$

$$h_l = c_{p,l}(T - T_m) + L + h_0 ,$$

$$h = fc_{p,l}(T - T_m) + fL + fh_0 + (1 - f)c_{p,s}(T - T_m) . \quad (9)$$

The choice of considering the specific heat capacity independent from the temperature is valid at the first order only in the proximity of the melting temperature. This was done for the sake of simplicity, even if future work could easily modify the numerical methods proposed in the present work to take into account the dependence of the temperature on the heat capacity.

Combining Eqs. (5), (6), and (9), and using the fact that $f = \frac{\rho_l}{\rho}g$ and $(1 - f) = \frac{\rho_s}{\rho}(1 - g)$, the volumetric enthalpy results in

$$H = \rho h = g\rho_l c_{p,l}(T - T_m) + (1 - g)\rho_s c_{p,s}(T - T_m) + g\rho_l L + \rho h_0 . \quad (10)$$

This quantity allows for writing the energy conservation equation in a simpler way. The energy conservation equation in a pure conduction situation reads

$$\frac{\partial H}{\partial t} = \nabla \cdot (k \nabla T) . \quad (11)$$

For a system undergoing a phase change, we can write H using the notions from CMT. It is noteworthy that, if we decide to express the volumetric enthalpy H as a function of the temperature T , the whole LHM is embedded in the time partial derivative term. Expanding the left side of Eq. (11),

$$\frac{\partial H}{\partial t} = \widehat{\rho c_p} \frac{\partial T}{\partial t} + \rho_l \lambda \frac{\partial g}{\partial t} , \quad (12)$$

where $\widehat{\rho c_p}$ and λ are defined as

$$\widehat{\rho c_p} := \rho_s c_{p,s} (1 - g) + \rho_l c_{p,l} g \quad (13)$$

$$\lambda := L + \frac{\rho}{\rho_l} h_0 . \quad (14)$$

Latent heat models differ from one another by the different approaches used to deal with the source terms. In general, the energy equation can be discretized, linearized, and numerically solved for the temperature T (temperature-based models), the volumetric enthalpy H , or the specific enthalpy h (enthalpy-based model). Since H depends on T , Eq. (11) is nonlinear.

Temperature-based latent heat methods introduce a closure relation to couple the two quantities and linearize the problem in T . Adopting the general notation proposed in Ref. [12], the discretized form of Eq. (11) is

$$a_p T_p = \sum_{nb} a_{nb} T_{nb} + d_p [H_p^0 - H_p] + b , \quad (15)$$

where

a_p, a_{nb} = matrix coefficients for the temperatures T_p and T_{nb} (respectively, for the current and the neighboring cells)

d_p = linear coefficients for the transient term multiplying the difference of total volumetric enthalpy for cell p between the previous and the current time step, H_p^0 and H_p

b = algebraic source term.

It is worth noting that even if the starting point was the conduction equation, Eq. (15) is the general discretized form of the energy equation. The convective term and any source term, once linearized in the temperature, can fit in this algebraic form of the temperature equation. Moreover, as it will be later presented in Sec. II.D, the velocity of the solid phase is assumed to be always equal to zero. This allows for simplifying the form of the convection term so that only the enthalpy of the liquid phase is convected. Since H_p depends on T_p and temperature-based methods linearize the problem in T and solve the discretized equation in T_p , this closure relation is adopted as

$$H_p - H_p^0 = S_p T_p + S_u . \quad (16)$$

The different T -based methods differ based only on the formulation of the source terms and the coupling algorithm between T and H . On the other hand, in H -based latent heat methods, the discretized energy equation will have a different formulation to accommodate the algebraic solution for enthalpy. In this work, only temperature-based methods were considered due to better compatibility with the current multiphysics solvers previously developed,^[16,17] in which the energy equation is solved in temperature. For this reason, two classic temperature-based methods have been implemented, namely, the AHC method and the ST method, along with a novel hybrid method. In the following section, the relationship between H and T is illustrated (closure relation). Afterward, the numerical models of latent heat are presented.

II.B. Closure Relations

All T -based latent heat methods are characterized by an energy equation with two coupled variables, T and g (T -based source term). These coupled variables introduce a nonlinearity into the equation, therefore closure equations are needed to link the two of them. Usually, it is assumed that locally the system lies on the H - T curve of the solid-liquid system. This is a simplifying assumption, since in general melting and solidification can be subjected to nonequilibrium phenomena, but the use of an equilibrium curve has the advantage of establishing a bijective relationship between the two quantities of interest, so that deriving one will automatically allow for establishing the other. Moreover, even under the assumption of equilibrium, enthalpy H depends also on other thermodynamical variables.

In the molten salt used in the MSR, there are different species, and their varying concentrations might affect melting and solidification. The modeling of the species concentration is beyond the scope of this work, and the salt will be considered a eutectic mixture that can be described only by the melting temperature T_m and latent heat L . For such isothermal-phase transitions, as a first approximation, one can consider a linear increase of enthalpy with temperature in the pure phases, with a jump discontinuity at the melting temperature. However, from the numerical point of view, introducing such a strong discontinuity poses stability issues, and therefore the phase change is smeared out into a finite interval of temperature. The discontinuity in the enthalpy field is now a weak constraint, as the enthalpy function is now continuous in temperature (with only its derivative discontinuous). This temperature interval is centered on the melting temperature T_m and is called a mushy zone. The variation of the enthalpy with temperature depends on the specific material, and the relations are based on semi-empirical models; once g and T are determined, all other quantities can be retrieved.

In the context of the MSFR, the mushy zone is not physical for what concerns isothermal transition. Therefore, the objective is to make this zone as small as possible, but large enough to have a well-behaved numerical solution. In this case, to mimic the presence of a small nonisothermal-phase transition, one can define a fictitious temperature of solidus T_s and liquidus T_l that are just a small distance ϵ away from the melting temperature, for instance by setting $T_s = T_m - \epsilon$ and $T_l = T_m + \epsilon$. The present work considered three simple closure relations; all three of them have a similar impact on the accuracy and stability of the solution, which is the desired outcome since they are just numerical tricks that must tend to the jump discontinuity in H - T . The first relation is a linear g - T relation (Fig. 1), defined as the following, where ϵ is a small temperature interval:

1. $g = 0$ for $T < T_m - \epsilon$
2. $g = 1$ for $T > T_m + \epsilon$
3. $g = \frac{T - T_m + \epsilon}{2\epsilon}$ for $-\epsilon < T - T_m < \epsilon$.

An optimal value of ϵ was found to be in the interval [0.1: 10 K]. The second relation is a variation of the previous one, using a sigmoid function centered in T_m for the variation of g , such that $g = 0.5$ when $T = T_m$ and $g = 0.99$ – 0.01 at $T = T_m - \epsilon$ and $T = T_m + \epsilon$, respectively.

The last closure relation that was tested was a linear H - T relation. The linear relation g - T automatically sets H to be a quadratic function of T in the mushy zone. To

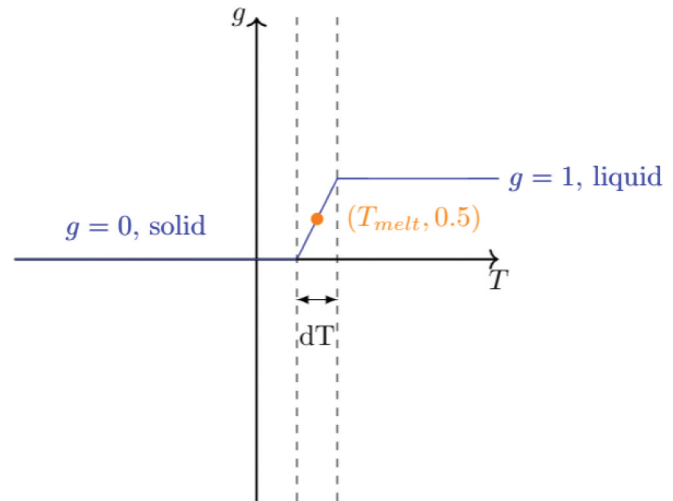


Fig. 1. Example of volume fraction g and temperature T closure relationship. The liquid fraction is 0 in the solid and 1 in the liquid. In the interval dT , the so-called mushy zone, the liquid fraction varies linearly between 0 and 1.

instead impose a linear relationship between H and T , the following is defined:

$$H_{pc} = \frac{dH}{dT_{pc}} T + H_{pc}^0, \quad (17)$$

where the subscript pc stands for phase change. Given the fictitious solidus and liquidus temperatures to be $T_s = T_m - \epsilon$ and $T_l = T_m + \epsilon$, respectively, the corresponding volumetric enthalpies are

$$\begin{aligned} H_s^* &= \rho_s c_{p,s} (T_s - T_m) = -\rho_s c_{p,s} \epsilon, \\ H_l^* &= \rho_l c_{p,l} (T_l - T_m) + \rho_l L = \rho_l c_{p,l} \epsilon + \rho_l L. \end{aligned} \quad (18)$$

Therefore,

$$\begin{aligned} \frac{dH}{dT_{pc}} &= \frac{H_l^* - H_s^*}{T_l - T_s} = \frac{\rho_l L + (\rho_l c_{p,l} + \rho_s c_{p,s}) \epsilon}{2\epsilon}, \\ H_{pc}^0 &= -\frac{dH}{dT_{pc}} T_s. \end{aligned} \quad (19)$$

II.C. Temperature-Based Models

II.C.1. Apparent Heat Capacity

The AHCs are the most straightforward way to implement latent heat in the heat equation. AHCs make use of the chain rule to approximate the total enthalpy time derivative:

$$\frac{\partial H}{\partial t} = \frac{\partial H}{\partial T} \frac{\partial T}{\partial t} . \quad (20)$$

Assuming the relation between H and T in time (for instance assuming thermal equilibrium) is known, the derivative $\frac{\partial H}{\partial T}$ can be evaluated at the previous time step, while the time partial derivative $\frac{\partial T}{\partial t}$ can be evaluated with the backward Euler method:

$$\frac{\partial H}{\partial t} \approx \frac{\partial H}{\partial T} \Big|_n \frac{T_p^{n+1} - T_p^n}{\Delta t} . \quad (21)$$

The algorithm runs as follows:

1. At the beginning of the time $t^{n+1} = t^n + \Delta t$, before the solution of the discretized energy equation, the temperature field is $T_p = T_p^n$, i.e., the temperature field is equal to the one calculated at time t^n .
2. The derivative $\frac{\partial H}{\partial T} \Big|_n$ is calculated from the temperature field T_p^n .
3. The energy equation is solved for the field T_p^{n+1} .
4. The calculation for the time t^{n+1} is concluded and one can move forward to the following time.

In this method, no iteration is needed to solve the nonlinearity between T and H . The coefficients in Eq. (16) are

$$S_p = \frac{\partial H}{\partial T} \Big|_n \quad (22)$$

$$S_u = -\frac{\partial H}{\partial T} \Big|_n T_p^n . \quad (23)$$

The AHC methods are easy to implement and fast running. However, the main drawback is that in some conditions, they could lead to an erroneous “skip” of the latent heat peak, which means that if the temperature has skipped from $T^n < T_s$ to $T^{n+1} > T_l$, or vice versa, the mushy zone is avoided. This drawback is usually overcome with the iterative ST at the expense of a higher computational cost.

II.C.2. Source Term Method

The ST is an iterative method that makes use of an inner loop for each time step. In addition to the classical outer loop for time discretization that it is used to solve

for the quantities at time t^{n+1} (as in the AHC method), an inner loop is used to solve for the nonlinearity between the temperature T and the volume fraction g . To do so, an iteration is carried out between the energy equation (that solves for T^{n+1}) and a formula for the update of the volume liquid fraction g^{n+1} to a new value $g^{n+1,*}$, which depends on the value of T^{n+1} calculated by solving the energy equation. Once the convergence for T^{n+1} and g^{n+1} is achieved for the inner loop, the other thermal quantities that depend on T and g are updated and we move to the new time step.

To use the ST, we need to calculate the temperature T by solving the energy equation as a function of the liquid fraction g . Hence, the volumetric enthalpy H (and more specifically, its partial time derivative) must be expressed as a function of the liquid volume fraction g and the temperature T , as in Eq. (12). Discretizing this latter relation and considering a slow variation of $\widehat{\rho c_p}$ and of λ with time, we get

$$\frac{H_p^{n+1} - H_p^n}{\Delta t} = \widehat{\rho c_p}^n \frac{T_p^{n+1} - T_p^n}{\Delta t} + \rho_l \lambda^n \frac{g^{n+1,*} - g^n}{\Delta t} . \quad (24)$$

Here, since both g and T are present at the same time t^{n+1} in the equation, we write $g^{n+1,*}$ to indicate that this quantity will be updated as a function of the temperature T_p^{n+1} in the inner loop. To obtain consistency between the two fields the following algorithm is used:

1. At the beginning of the time $t^{n+1} = t^n + \Delta t$, before the solution of the discretized energy equation, the temperature field is $T_p^{n+1} = T_p^n$, i.e., the temperature field is equal to the one calculated at time t^n , and the same holds for g , i.e., $g^{n+1} = g^n$.
2. The energy equation is solved for the field T_p^{n+1} .
3. The liquid fraction is updated with the following formula:

$$g_p^{n+1} = g_p^{n+1,*} + \frac{\widehat{\rho c_p}}{\rho_l L} (T_p^{n+1} - T_m + \epsilon - 2\epsilon g_p^{n+1,*}) , \quad (25)$$

which is a proposed extension of the formula commonly used for constant thermophysical properties (e.g., in Ref. [26]), extended for different thermophysical properties between the solid and liquid phases.

1. The liquid fraction is limited between 0 and 1: if $g_p^{n+1} < 0$, then $g_p^{n+1} = 0$; if $g_p^{n+1} > 1$, then $g_p^{n+1} = 1$.

2. Check if convergence on the fields g and T is reached; if not, reset the value of $g_p^{n+1,*} = g_p^{n+1}$ and go back to step 2.

3. If at step 5 both g and T are converged, the calculation for the time t^{n+1} is concluded and one can move forward to the following time.

As can be seen from the formulation of the algorithm, steps 2 to 5 can be considered an inner phase-change loop.

The ST in general is accurate and does not suffer from the problem of latent heat peak skipping, unlike the AHC method. On the other hand, it is much slower than the AHC method, being iterative and slowly converging. To combine the advantages of both methods, a hybrid approach is proposed in the next paragraph. In fact, we exploit the fact that in this formulation of the ST, we can reduce Eq. (24) to the more generic formulation of Eq. (16), where the coefficient S_p corresponds to all the terms multiplying T_p^{n+1} , becoming an addend to the diagonal of the matrix of the discretized energy equation, while all other terms go under S_u . This fact allows for easily writing a generic form of the T -based energy equation valid both for the AHC method and ST method, so that an algorithm that can allow for switching at run time from one method to the other just by changing the evaluation of S_p and S_u .

II.C.3. Hybrid Method

A novel T -based approach to the LHM is proposed, which is called the “hybrid approach” because it brings together the two existing T -based latent heat models (i.e., the AHC method and the ST method), exploiting the complementary strengths and weaknesses of the two, thus increasing computational efficiency and robustness. On the one hand, the fact that the temperature-based discretized energy equation has the same form independently of the latent heat model used allowed for the implementation of only one T -based solver. In fact, by choosing the appropriate coefficients S_p and S_u in Eq. (16) and a closure relationship, one can select and even modify the latent heat model at run time. This was found to be particularly convenient to combine the strengths of the two models in a single hybrid model, reducing their inconveniences. The hybrid model can be presented in the following way:

1. Start the time-step calculation as the AHC model until the solution of the energy equation.

2. After the solution of the energy equation, check whether the new temperature field has “skipped” the latent heat peak, i.e., whether in any cell the temperature has skipped from $T < T_s$ to $T > T_l$, or vice versa, avoiding the mushy zone.

3. If the latent heat peak has been skipped, the temperature field is taken back to the value that it had before the solution of the energy equation, i.e., to the value of the beginning of the time step.

4. If the latent heat peak has been skipped, the latent heat model is changed to the ST one, iterating between the energy equation and the closure relation in the phase-change loop until convergence.

5. Go to the next time and start the algorithm again.

The combination of the two algorithms allows for exploiting the speed of the AHC method, using it until it fails to include the latent heat peak, in which case the ST method is used to achieve better robustness, using the increased stability with the iterations of the phase-change loop. This was found to be a good compromise between robustness and speed.

II.D. Velocity Transition Modeling

The other main phenomenon in melting and solidification processes is the VTM. As the solid and the liquid phases respond differently to imposed shear stresses, the velocity field must consider this discrepancy. In practice, fixed-grid methods do not implement explicitly the mechanical aspects of the interactions between phases; instead, they modify the classical Navier-Stokes equations for the liquid phase by setting the velocity field equal to a constant in the solid domain, neglecting all mechanical aspects of the system.^[11] An additional simplification will be assumed, i.e., the solid phase is considered to be still, so that only the liquid phase is allowed to displace, and the velocity in the solid phase must be equal to zero.

The most popular method for VTM is the DST method, which adds a source term in the Navier-Stokes equations that vastly exceeds the values of all other terms in the equation for the cells in the solid domain, thus forcing the velocity to be zero, while approaching zero in the liquid domain:

$$\vec{F} = \frac{(1-g)^2}{g^3 + \epsilon} C v \vec{u} , \quad (26)$$

where C is the Darcy constant and v is the kinematic viscosity. This method allows for a smooth transition of the velocity from solid to liquid with minimum implementation effort.

To solve for the velocity and the pressure field, we make a simplifying assumption to justify the use of the incompressible Navier-Stokes equations. In particular, on one hand, we leverage the work of Ref. [10] in which the impact of higher-order terms on the dependency of the density from the temperature and solute concentration has been studied. It has been demonstrated that the solenoidal condition for the liquid velocity field \vec{u}_l is appropriate for context in which the temperature of the salt is up to 40 K above the eutectic, while it is true that the impact of the solute-driven convection is important very close to the interface. Moreover, one extra argument that can be used to relax a bit the domain of applicability of the incompressible approximation is the quasi-static nature of the fluid dynamics with respect to the melting dynamics; this justifies the use of $\nabla \cdot \vec{u} \approx 0$ for each fluid dynamical time step. In the present work, we do not take into account the chemical composition of the salt and the modeling of the solute concentrations. If a more precise description of the buoyancy terms is needed in the future, one can consider implementing higher-order terms.

In conclusion, the pressure and velocity field are solved by means of the classical methods used for the Navier-Stokes equations, which are coupled to the energy equation by the DST. The effects of natural convection are modeled through the Boussinesq approximation.

III. MODEL VERIFICATION

As mentioned in Sec. II, the solvers implemented in OpenFOAM are meant to deal with both conductive and convective problems, with the possibility of choosing one of the latent heat models proposed, i.e., AHC method, ST method, or the developed hybrid one (Table I). In this light, the three latter modeling options are tested against two verification cases: a pure conductive one-dimensional (1-D) slab case and a conductive-convection two-dimensional (2-D) square case.

III.A. Conduction Case

Verification of the conduction solvers was carried out by comparing the results with the analytical solution of the

two-phase Stefan problem, as suggested in Ref. [8]. The most basic mathematical description of melting and solidification phenomena is due to Josef Stefan,^[27] and the respective mathematical problem is indeed known as the Classical Stefan Problem.^[7] The unknowns of this problem are the temperature field and the position of the interface between solid and liquid. One of the most interesting aspects of the problem is its nonlinearity, meaning that the position of the interface depends on the temperature, and vice versa. Such a nonlinearity is further complicated by the fact that a condition enforcing an “energy conservative” heat flux must be put on the interface in order to keep into account the latent heat exchanged between solid and liquid.

The Stefan problem has an analytical solution only in a 1-D configuration; it is the melting of a semi-infinite slab $0 < x < \infty$, initially solid at temperature $T_s < T_m$, by imposing a constant temperature $T_l > T_m$ on the face $x = 0$, with all thermophysical parameters constant. Mathematically, the problem requires finding a temperature distribution $T(x, t)$ and an interface position function $X(t)$. The mathematical details are already well known in the literature, and a complete explanation of the problem can be found in Ref. [8].

The conduction solver was verified using the Stefan problem, considering a finite slab, initially solid at a temperature $T_s < T_m$, heated from one side by imposing a fixed temperature $T_l > T_m$, while the other is adiabatic. Being that Neumann’s solution is valid only for a semi-infinite slab, the numerical solution will accumulate an amount of difference compared to the analytical solution as the time increases. However, for instants at which the heat flux of the analytical solution at $x = l$ is still sufficiently small, the difference between the analytical and the numerical solution is negligible and will depend only on the accuracy of the numerical method.

III.A.1. Case 1: $\rho_l = \rho_s$; $c_{pl} \neq c_{ps}$

Case 1 is depicted in Fig. 2, whereas the parameters of the case are given in Table II. The AHC method and ST method are compared against the analytical solution of the temperature at $t = 1000$ s in Fig. 3 with remarkably good agreement. A good agreement between the numerical and

TABLE I
OpenFOAM Solvers Implemented

Name	Conduction	Convection	Radiation	LHM	VTM
meltingTConduction	Yes	No	No	AHC/ST/Hybrid	No
meltingPimpleFoam	Yes	Yes	No	AHC/ST/Hybrid	DST

$$T(x = 0, t) = T_m + 20^\circ C \quad \bullet \xrightarrow{T(x, t = 0) = T_m - 13.15^\circ C} \bullet \frac{dT(x = L)}{dx} = 0$$

Fig. 2. Depiction of case 1.

TABLE II
Case 1 Parameters

Property	Value
c_{ps}	2 040 J kg ⁻¹ K ⁻¹
c_{pl}	4 186 J kg ⁻¹ K ⁻¹
ρ	1 000 kg m ⁻³
k	0.6 W m ⁻¹ K ⁻¹
Latent heat	334 000 J kg ⁻¹
T_m	273.15 K
T_s	260 K
T_l	293.15 K
Slab length	0.1 m
Number of cells	25, 50, 100
Numerical time step	0.1, 0.5, 1
dT	0.1, 1

analytical solution is reached, both for the temperature field and the interface position, as seen in Figs. 4 and 5. The solution is shown to be consistent for different meshes (Fig. 4) and time steps (Fig. 5). In addition, the choice of the algorithm for the latent heat model does not influence meaningfully the accuracy of the solution if convergence is achieved and if a correct time step and width of the mushy zone are chosen to ensure energy conservation.

However, it can be seen that the AHC can suffer a loss of accuracy for some values of the numerical parameter dT , in particular in this case when $dT < 1$ K (Fig. 6), since dT for isothermal transitions is not a physical parameter, and hence its value is not easy to choose a priori before launching a calculation. This effect is even greater for calculations with higher thermal flux, as is shown in the next case.

III.A.2. Case 2: $\rho_l \neq \rho_s$; $c_{pl} \neq c_{ps}$

Case 2 is depicted in Fig. 7, whereas the parameters of the case are given in Table III. In this case, the properties of the materials are equal to the LiF₄ salt, which is used in nuclear applications and has different solid and liquid densities. For this configuration, the choice of the LHM and its numerical parameters will highlight the characteristics of each of these methods; using a mushy zone interval of 0.1 K, the AHC brings to a latent heat peak skipping (Fig. 8), and the agreement with the analytical solution is compromised for the beginning of the transient (where the gradient is steeper), leading to a shift in the numerical solution. On the contrary, the ST is consistently close to the analytical solution. As the latter is an iterative method, convergence was considered

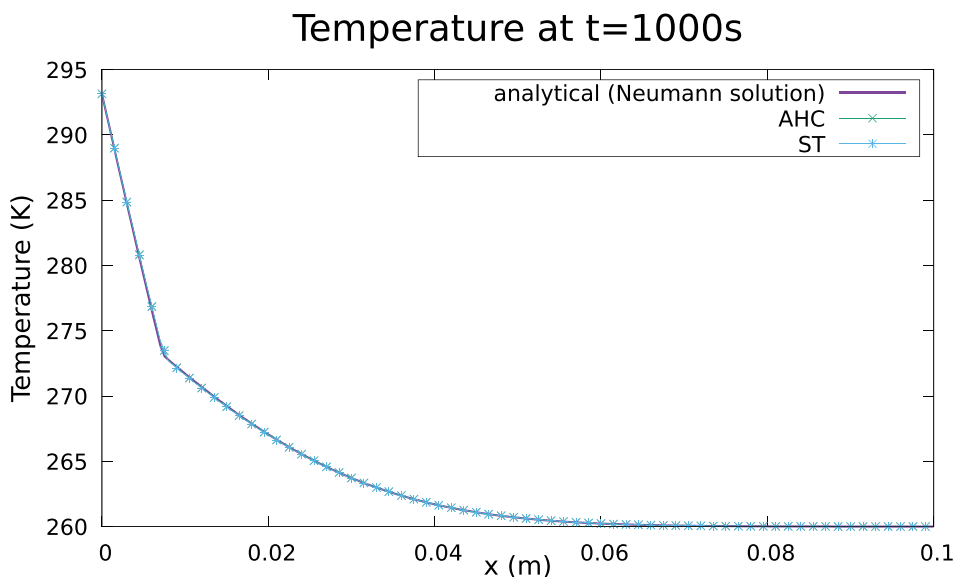


Fig. 3. Temperature field at time $t = 1000$ s (mesh = 100 cells).

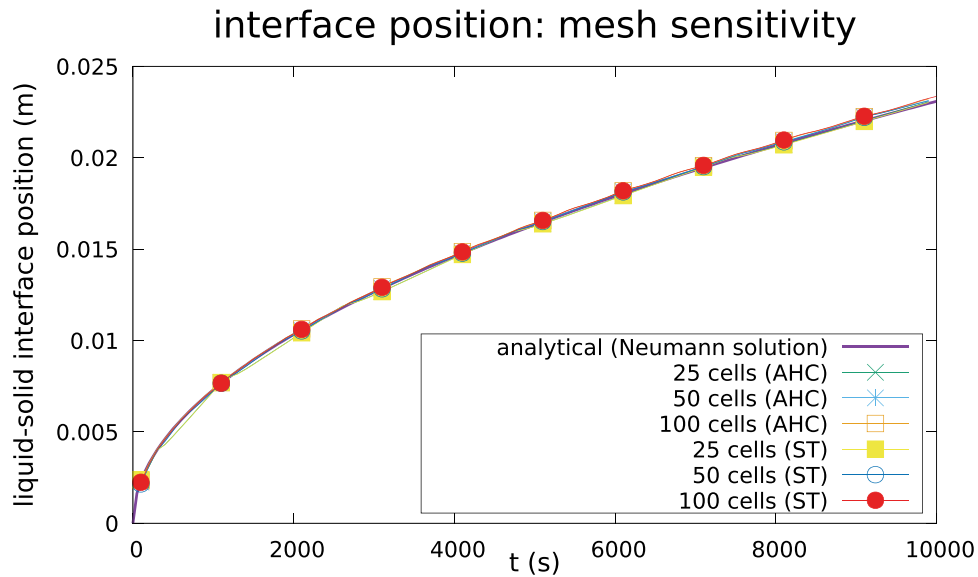


Fig. 4. Mesh sensitivity for the 1-D case (time step = .1 s).

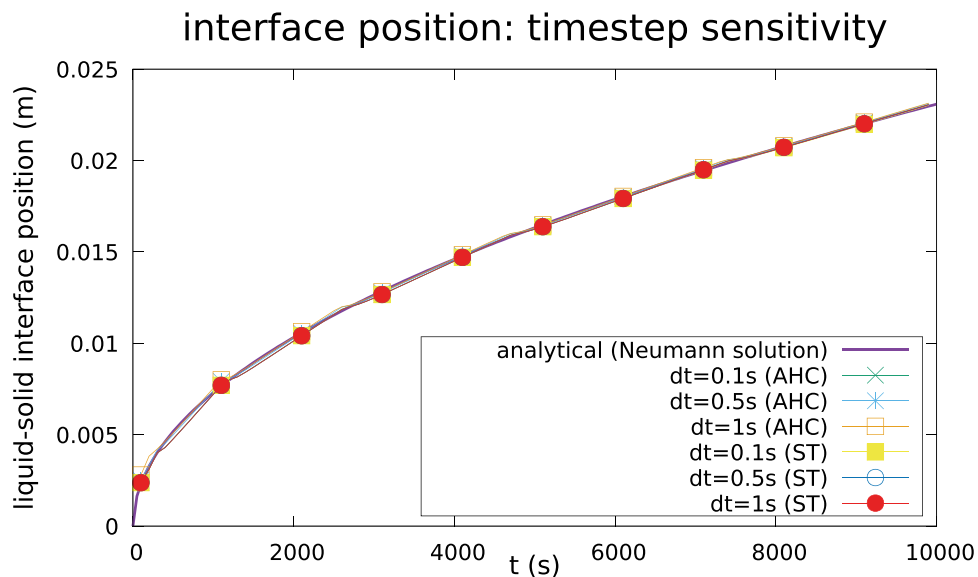


Fig. 5. Sensitivity to different time steps for the 1-D case (mesh = 25 cells).

achieved when the L^2 residual norm of both the g and T fields were below 10^{-5} .

The outcome is that the ST leads to more accurate results at a much slower cost since, on average, around 20 iterations per time step were required for convergence. The dynamic choice of the latent heat model with the hybrid algorithm (AHC + ST) can avoid inaccurate results as it changes the LHM to the ST for all those times in which the peak skip happens with the AHC. With this approach, a good agreement with the reference solution was achieved, with an execution speed

comparable to the AHC. The execution times are compared in Fig. 9.

An accurate solution can be obtained also with the AHC by fine-tuning the choice of the width of the mushy zone. With a mushy zone of $dT = 1$ K, a good agreement with the solution can be obtained (Fig. 10). However, selecting an appropriate value for the dimension of the mushy zone can be tricky, especially using the AHC, since there are no prior considerations that can be made to be sure that the result will take into account the latent heat. On the contrary, the hybrid approach is much less

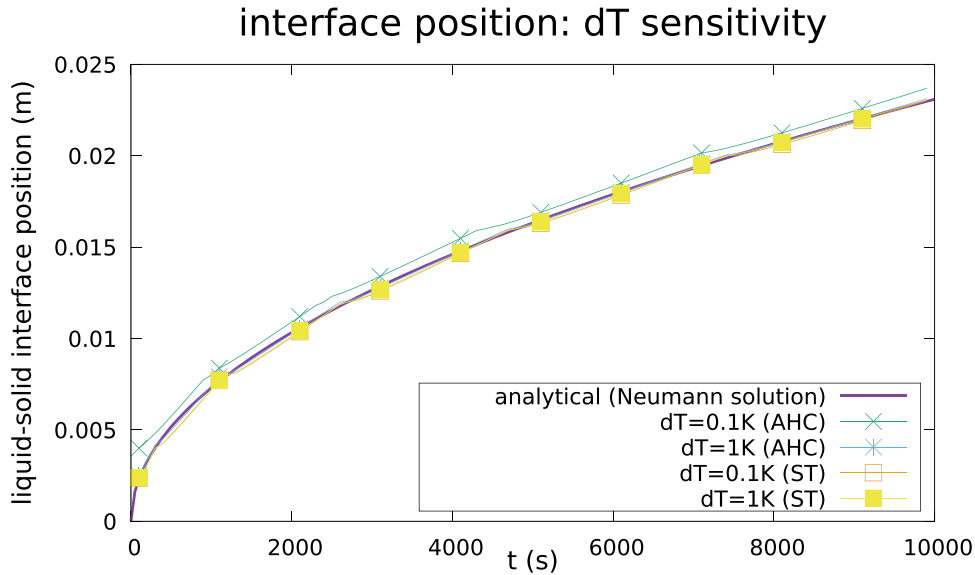


Fig. 6. Sensitivity to the parameter dT of the latent heat models for the 1-D case (mesh = 25 cells, $dT = 0.5$ s). It can be seen that the AHC model suffers a loss of accuracy for $dT < 1$ K.

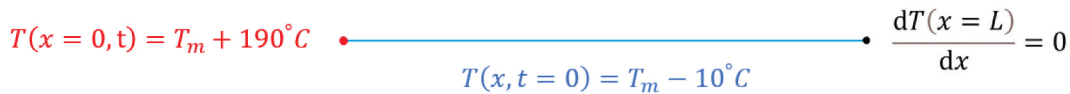


Fig. 7. Depiction of case 2.

TABLE III
Case 2 Parameters

Property	Value
c_{ps}	815 J kg ⁻¹ K ⁻¹
c_{pl}	1 000 J kg ⁻¹ K ⁻¹
ρ_s	4 502 kg m ⁻³
ρ_l	4 390 kg m ⁻³
k	1.5 W m ⁻¹ K ⁻¹
Latent heat	159 000 J kg ⁻¹
T_m	841 K
T_s	831 K
T_l	1 031 K
Slab length	0.1 m

sensitive to the choice of the mushy zone width, while ensuring a good compromise between solution accuracy and speed. The code has been verified also in a 2-D square geometry, obtaining similar results

III.B. Convection Case

For verification of the convective solver, the numerical solution found in Ref. [25] was used as a reference. The

case consists of a cavity of tin, initially solid at $T = T_m$, heated from one side by setting the temperature of the left wall at $T_l > T_m$ (Fig. 11). The cavity is a square with a side equal to 0.1 m. The mesh is an orthogonal 100×100 cell in the x - and y -directions, with a $7 \times$ grading in the x -direction (Fig. 12). As the layer of liquid keeps growing from left to right, the convective motion created by buoyancy becomes stronger and stronger, influencing the shape of the melting front. The resulting flow pattern is laminar and multicellular in nature (i.e., has a structure formed by multiple laminar eddies).

The material properties are the ones from Ref. [25]. The hot wall is set at a temperature 3°C greater than the initial solid temperature, which is at a temperature lower than the melting temperature to accommodate the existence of the mushy zone; the chosen mushy zone is 0.1°C thick and the initial temperature of the solid cavity is set to be 0.05°C under the melting temperature ($T = 504.95$ K, $T_m = 505$ K, and $T_h = 508$ K). The numerical schemes used are second-order accurate, and the pressure velocity coupling is solved using the Pressure-Implicit with Splitting of Operators (PISO) algorithm.

The case couples both the convective part and the conduction, which is relevant for the MSFR case

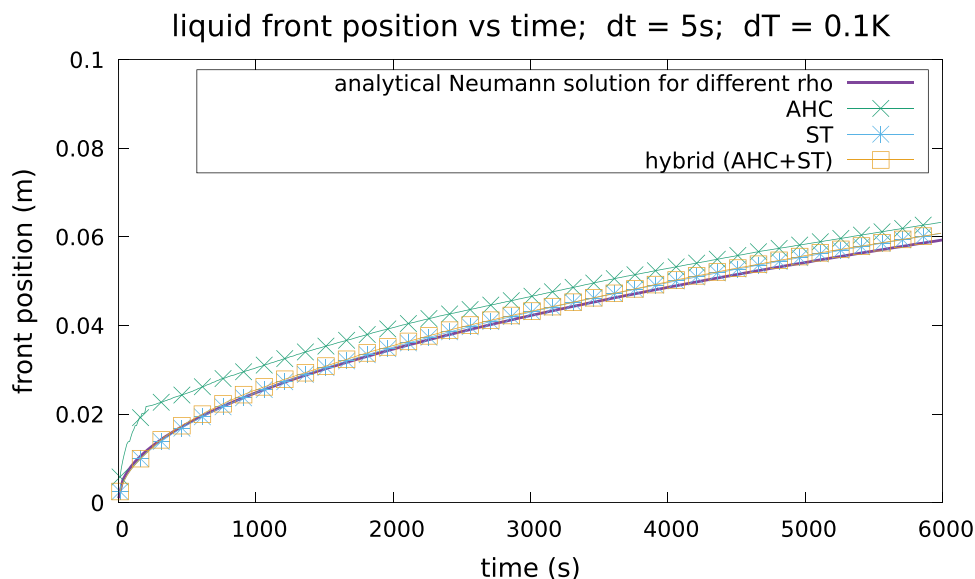


Fig. 8. Interface position for case 2. With a mushy zone of 0.1 K, the AHC can fail to take into account the latent heat if the dT is too small, while the ST and hybrid methods guarantee better agreement with the analytical solution.



Fig. 9. Execution times for the two cases: for a small computational cost, the hybrid AHC + ST can improve precision (serial execution on desktop PC with Intel(R) Core™ i7-6700HQ CPU at 2.60 GHz, 4 GB DDR4 RAM).

(Fig. 13). The reference solution was obtained using an enthalpy source latent heat model, which is an interesting comparison since the convection solver developed in the present work is temperature based. It can be seen that the source method is a little more in line with the reference solution (Fig. 14). On the other hand, the AHC is slightly underestimating the interface position, while being faster. With such a small temperature gradient, the AHC does not have problems with peak skipping, so the hybrid approach is equivalent to the AHC.

IV. APPLICATION TO MOLTEN SALT FREEZE VALVES

As mentioned in Sec. I, one of the main reasons for MSR analysis to model melting and solidification phenomena is the study of the freeze plug. The freeze valve will be essentially a section of a draining pipe with salt in it. In its closed state, a solidified salt prevents the fuel salt from draining, while in the open state, the melting of the freeze plug allows for the discharge of the fuel salt into an emergency tank. The general idea is that in normal

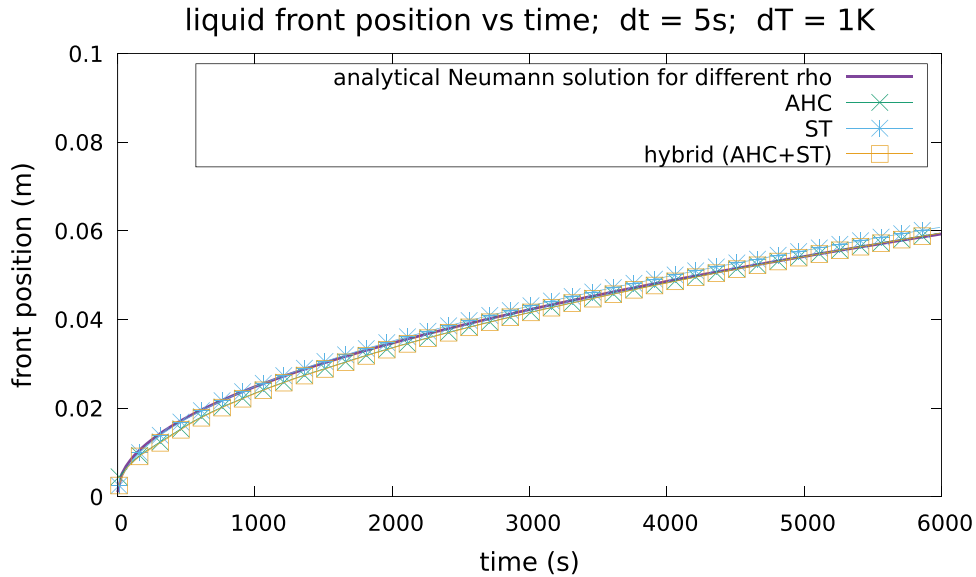


Fig. 10. Interface position for case 2 with a mushy zone of 1 K. All three models are in good agreement, as the use of a larger dT helps stabilize the AHC. However, the bigger the dT , the farther the case is from an ideal isothermal transition.

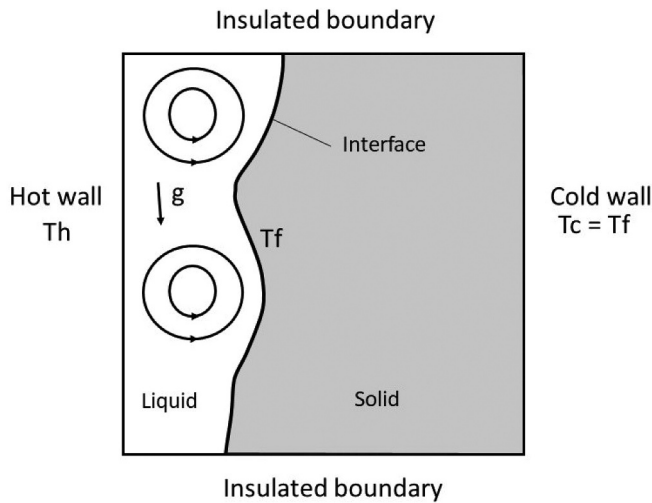


Fig. 11. Verification case for the convection solver. The temperature left wall of the 2-D cavity is set to a value greater than the melting temperature. The emerging flow pattern is an effect of buoyancy.^[25]

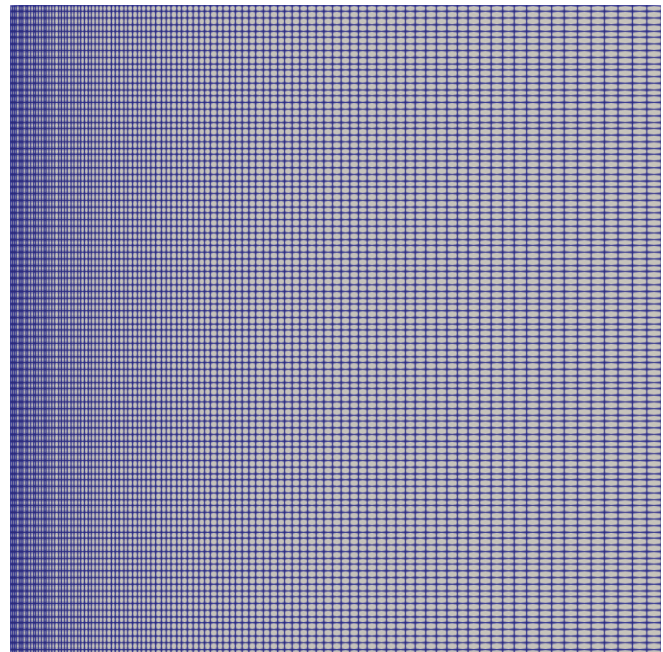


Fig. 12. Computational grid of the 2-D buoyancy-based case consisting in a 100×100 mesh with a $7 \times$ grading in the x-direction.

conditions, a portion of the draining pipe is cooled to guarantee a closed state of the valve. On the contrary, given an accident scenario, the rise in temperature in the core (and the interruption of the valve cooling) should initiate a melting in the frozen valve, eventually leading to the opening of the valve.

In the MSFR, the exact mechanisms of the opening of the valve are still to be investigated and optimized. On the one hand, if the configuration of the valve is such that, after a certain degree of melting, the hydrostatic

pressure is enough to mechanically push the solid plug out of its position and allow for the flow of the liquid, then the opening condition should be investigated in the framework of a thermo-fluid-mechanical analysis. On the other hand, if the configuration of the valve does not provide for a mechanical displacement of the plug, melting will be the dominating phenomenon for the opening

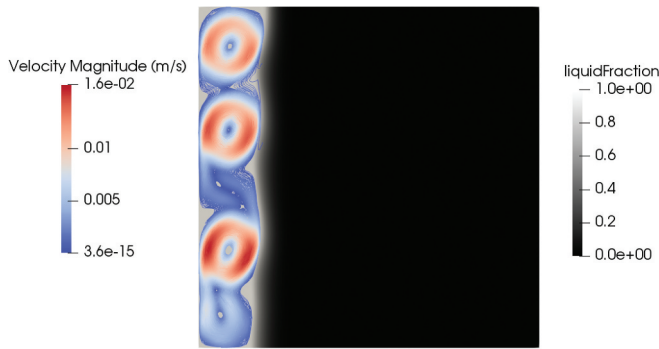


Fig. 13. Buoyancy-induced multicellular pattern development in the melted zone ($t = 450$ s; black is solid).

of the valve. In the first case, the analysis should focus on the melting of the salt near the wall and how much it affects the mechanical resistance of the valve. In the second case, the shape of the solid-liquid interface, and hence, the heat transfer, will probably be the main factor regulating the dynamic of the valve. The latter was considered in the present study.

A simple trial configuration was chosen to test the code in a case with conditions that are as close as possible to a real system. The chosen geometry was a simple cylinder, representing the section of the draining pipe occupied by the valve (Fig. 15).^[15] The boundary conditions were selected knowing that the position of the valve in the reactor should be at the bottom of each heat exchanger leg. This implies that in nominal working conditions, the temperature at the top face of the valve

is around 650°C , while the sides are cooled to a temperature lower than the melting temperature. The subcooling of the valve is one of the key parameters influencing the melting time; in the present work, it was assumed to be 5°C , so with the melting temperature being 568°C , the temperature imposed on the side walls of the valve was 563°C (when the cooling was active). The numerical simulations used a mesh (Fig. 16) formed by 120 400 hexahedral elements, with boundary layer refinement on the side wall to account for the steep gradients in this region.

According to the accident scenario and mechanism activation of the freeze plug, the boundary conditions may change. Two different transient scenarios were modeled. In the first case, the cooling of the valve was switched off (for instance, during a power outage), making the side walls of the valve adiabatic. Considering the recommendations in Ref. [4], a value of 1000°C was imposed at the top face to consider the maximum temperature that builds up during either a loss of heat sink (LOHS) or a loss of fuel accident.

In the second case, a more complex boundary condition was taken into account. As can be seen in Ref. [4], at least when only pure conduction is considered, the melting of the plug can be very slow (longer than 1000 s). A possible solution to the problem is to add a conductive material attached to the wall of the draining pipes, so that it can conduct heat much more rapidly on the side wall of the plug, making it easier to melt close to the walls and eventually helping the displacement of the plug.

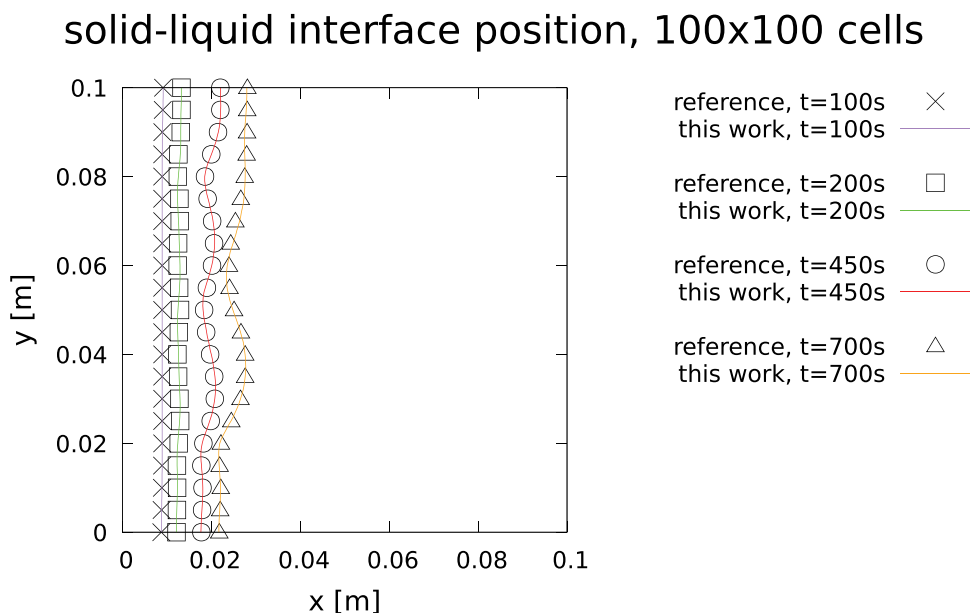


Fig. 14. Position of interface with respect to the reference solution.

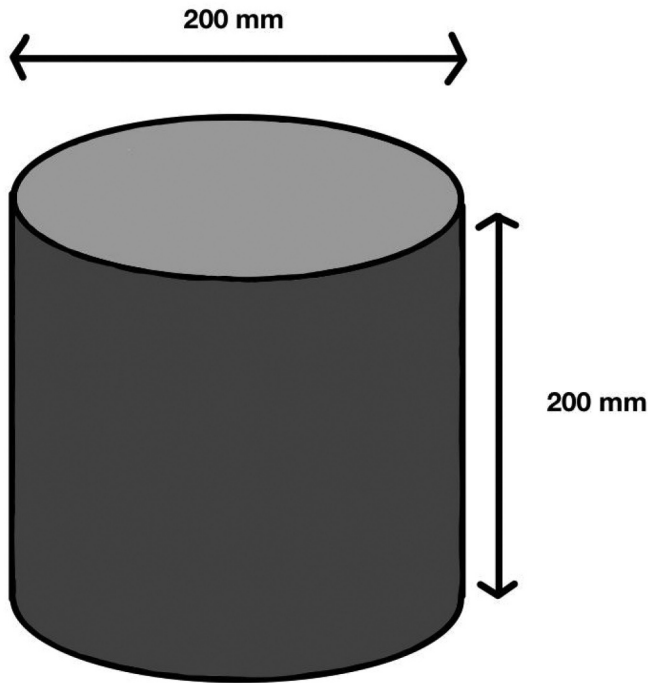


Fig. 15. Dimensions of the section of the pipe considered in the analysis.

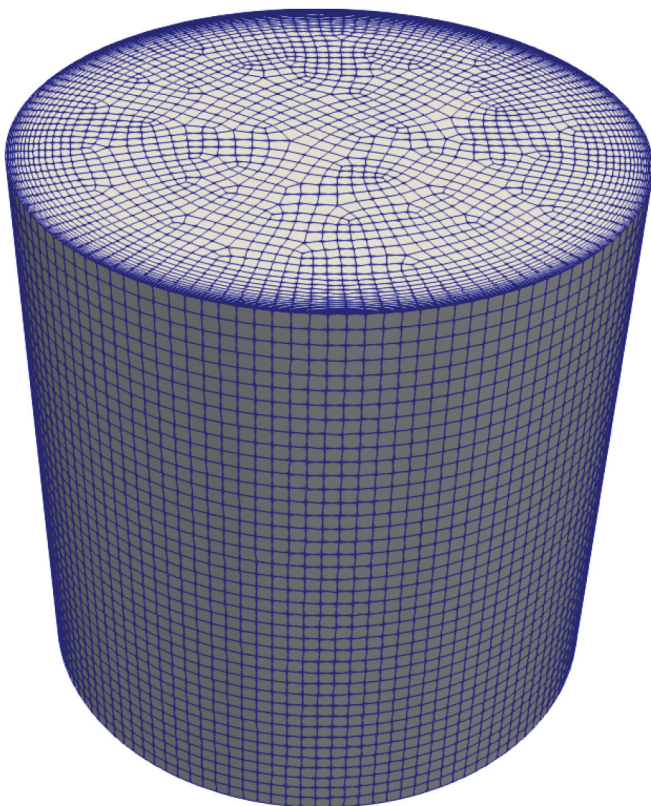


Fig. 16. Three-dimensional mesh for the plug.

Modeling such a multicomponent system requires a multiregion approach.

Given the single-region nature of the developed code, a case that mirrors the presence of a metal mass around the tube has been set up through appropriate boundary conditions and a 1-D approach by considering a semi-infinite slab of metal surrounding the plug, starting from the upper surface of the valve and going downward. This slab is initially at $T = 563^\circ\text{C}$. At $t = 0$, the upper surface of the valve and of the metal rise to 1000°C . Due to axial conduction, the metal slab heats up progressively, imposing a temperature boundary condition on the salt cylinder, which is a function of the axial coordinate and of time and coincides with the solution of the heat conduction equation for a semi-infinite slab stated as follows:

$$\begin{aligned}
 T_t &= \alpha T_{xx}; \quad 0 \leq z < \infty; \quad t > 0, \\
 T(z, 0) &= T_0; \quad 0 \leq z < \infty, \\
 T(0, t) &= T_H; \quad \lim_{z \rightarrow \infty} T(z, t) = T_0; \quad t > 0, \\
 T(z, t) &= T_H - (T_H - T_0) \operatorname{erf}\left(\frac{z}{2\sqrt{\alpha t}}\right), \quad (27)
 \end{aligned}$$

The last part of Eq. (27) is the boundary condition imposed on the side wall of the cylinder if the z -axis starts at the upper face of the valve and is directed downward. In all cases, the lower wall of the valve was taken as adiabatic. The cases with the temperature boundary conditions are summarized in Table IV.

All three cases were considered using both the solver for pure conduction and the one included also for convection. The former represented the most conservative approach, neglecting all movements of the liquid phase. In the latter case, the valve was positioned close enough to the reactor to be affected by the influence of salt circulation.

TABLE IV

Temperature Boundary Conditions for the Three Case Studies of the MSFR Freeze Valve

Case	Cylinder face	Temperature Boundary Condition
Steady state	Top	Fixed temperature $T = 650^\circ\text{C}$
	Side	Fixed temperature $T = 563^\circ\text{C}$
	Bottom	Adiabatic
Transient 1	Top	Fixed temperature $T = 1000^\circ\text{C}$
	Side	Adiabatic
	Bottom	Adiabatic
Transient 2	Top	Fixed temperature $T = 1000^\circ\text{C}$
	Side	Variable temperature $T = T(z,t)$
	Bottom	Adiabatic

This can be significant, for instance, in a LOHS scenario in which the pump keeps working, and hence salt circulation in the core is still present, or in cases in which the design of the reactor is such that it allows for natural circulation, also in the case of a loss-of-offsite power scenario.

As will be shown, forced convection had a huge impact both on the shape of the melting interface and on the melting time. As a first approximation of the forced convection induced by the motion of the salt in the primary system, the top wall was set to a moving wall with constant velocity along the x -axis equal to 0.1 m/s, which is compatible with the maximum velocity in the core (between 1 to 5 m/s), assuming a velocity one order of magnitude lower due to the proximity of the walls. In addition to forced convection, the contribution of natural circulation also was considered, but its influence turned out to be completely negligible. This means that, for what concerns the geometry used in the present study, natural circulation inside the valve did not have any significant impact.

IV.A. Steady-State Results

Steady-state simulations were performed as the first step to investigate the presence of a stationary solution with the boundary conditions defined in Table IV. This kind of simulation can be used to assess if a design complies with the requirement of having a closed valve during normal operations.

A first simulation was performed with the only-conductive solver. In this case, the position of the interface location (Fig. 17) adapted to the shape of the temperature field that developed in the valve (Fig. 18). The valve could

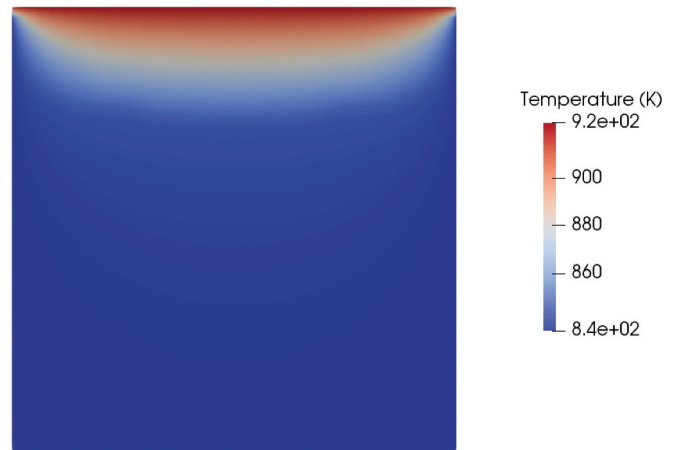


Fig. 18. Temperature field at steady state (conduction).

be considered closed since the solid plug impeded the flow of the upper liquid to the lower face.

The same case was performed with the meltingPimpleFoam solver (see Table I) using the hybrid approach as a latent heat model. Setting a velocity on the top wall equal to 0.1 m/s, a stationary solution in the laminar regime did not exist. However, even if the flow pattern is oscillatory, since the melting dynamics is much slower than the fluid dynamics, the solid-liquid interface is on average stable in the same position at around 700 s of physical time. Including the effects of forced convection, the shape of the melting front changed compared to the case of pure conduction (Fig. 19). While the position of the melting front at the centerline of the cylinder was similar (0.14 m for conduction and 0.12 for convection starting from the bottom face), the thickness of the melting front near the wall was much thinner in the case of forced convection, and the same held for the

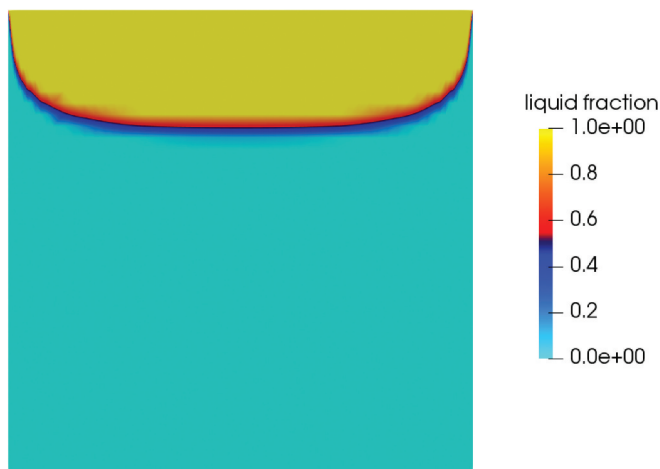


Fig. 17. Section at the midplane of the valve; liquid fraction position at steady state for pure conduction.

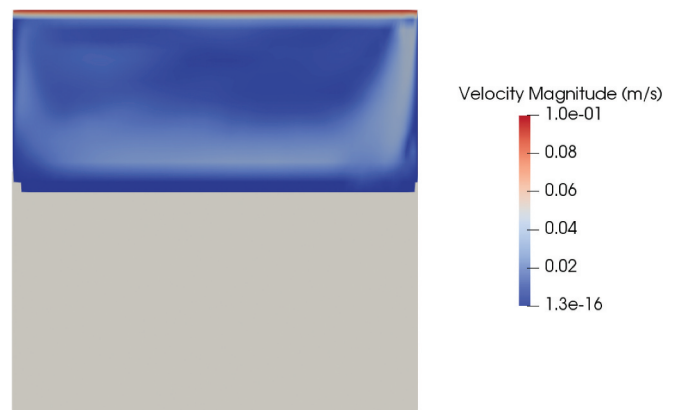


Fig. 19. Section at the midplane of the valve; liquid fraction position at steady state with convection (white is solid and blue is liquid) and visualization of the velocity field in the liquid.

total liquid fraction on the valve (0.21 for conduction and 0.38 for convection). This result proves that, if the valve will rely on mechanical working principles, the thickness of the solid near the walls will be an important parameter to assess the mechanical resistance of the valve and its capability of holding the hydrostatic pressure of the reactor salt. The reason for the difference in the melting front shape is that the convection of energy evens out the temperature field in all the liquid regions (Fig. 20).

IV.B. Transient Results

The time-dependent analysis was aimed at calculating the time required by the freeze plug to melt and then drain the fuel salt. The initial condition was retrieved from the stationary solution presented in the previous section. At time $t = 0$, the temperature of the top face of the wall was brought to 1000°C , while the cooling on the sides of the valve was switched off.

First, the case with the adiabatic walls is considered. The evolution of the melting front in the case of pure conduction had a very simple behavior in terms of shape. After the first few tens of seconds, the U-shaped front of the steady state was flattened to a straight shape in which the front proceeded parallel to the top surface. The time of melting for this transient in pure conduction was beyond 10 000 s. This time was way beyond any acceptable limit for the activation of the draining in the reactor core, and this result is in agreement with previous works on freeze valves that suggested that for their use in a passive way with the decay heat from the core to melt the valve, some systems that aid the heat transfer will be required (Fig. 21).^[4]

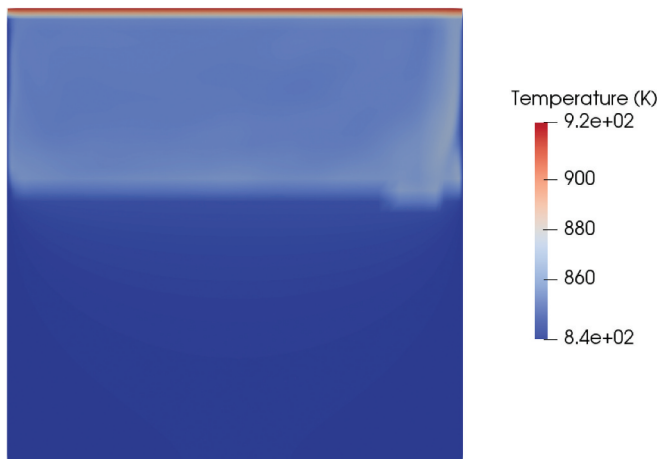


Fig. 20. Temperature field at steady state (convection).

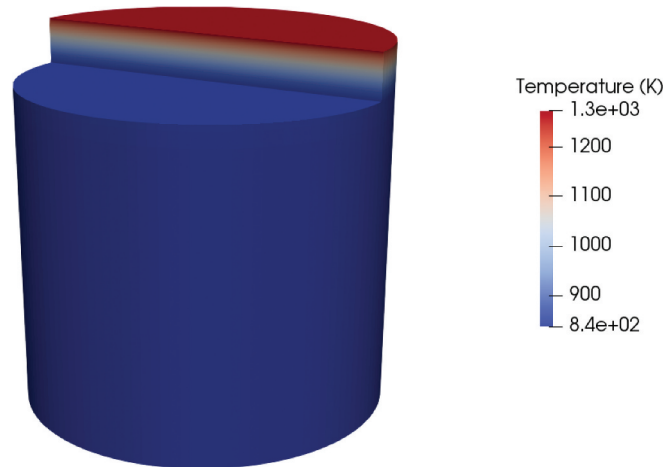


Fig. 21. Temperature field (K) and melting interface in pure conduction (500 s) and adiabatic walls.

Considering also the convection of the fluid, the melting time changed dramatically (Fig. 22). The much more efficient heat transfer in this case led to a much more even temperature profile in the liquid, reducing stratification. This translated to a huge difference in the melting time since for the forced convection case, the first portion of the liquid reached the bottom surface in 920 s, one order of magnitude faster compared to the conduction case. However, this time likely will be too high to guarantee good use of the passive draining system, as it is quite close to the upper recommended limit of 1000 s.^[4] Still, this result proved that in the case of LOHS both in the core and in the valve, convection, when present, plays a dominant role in the melting time, and as a consequence, in the opening of the valve.

The same transient was performed considering some more realistic boundary conditions with a variable temperature on the side wall (Table IV). These conditions mimicked a mass of metal (Hastelloy, Table V) surrounding the valve and conducting heat from the upper part of the valve (close to the reactor, at 1000°C) to the lower part. A similar configuration can be found in Ref. [4] in which the valve was positioned in a metal tube heated from above. As for the previous transient, the case was initialized starting from the steady-state solution, both for conduction and convection.

For pure conduction, a peculiar shape of the melting front was produced for both the pure conductive and the convective cases (Figs. 23 and 24, respectively). With the side wall progressively heating, the temperature in the salt near the wall rose faster than the central part of the plug. This created a layer of the melted area that made the solid detach from the side

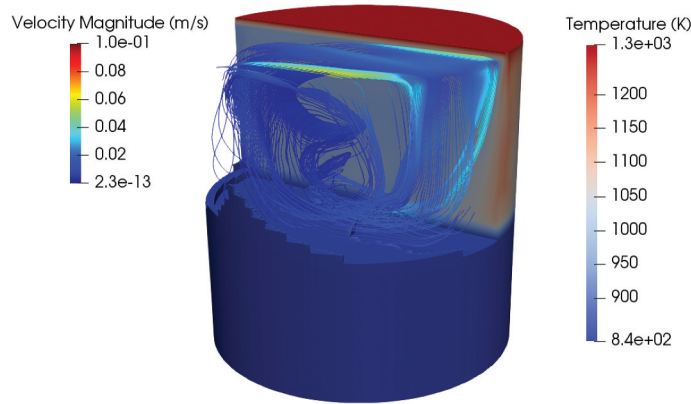


Fig. 22. Temperature field (K) and melting interface with convection (500 s) and adiabatic walls. The streamline pattern is visualized.

TABLE V

Thermal Properties of the Hastelloy

Property	Value
ρ	8860 kg m ⁻³
c_p	578 J kg ⁻¹ K ⁻¹
k	23.6 W m ⁻¹ K ⁻¹

Adding convection, both the shape of the melting front and the melting times were dramatically different from those of the case of pure conduction. The shape of the melting front was influenced by the “erosion” caused by the enhanced heat transfer due to convection (Figs. 24 and 25).

A mesh sensitivity analysis was also performed on transient 2 to test the influence of the computational grid on the results. Two additional meshes were adopted, i.e., the first one was obtained by refining the mesh only in the *z*-direction (doubling the cells) and the second with a refinement in all directions, leading to an increase by a factor 8 of the number of cells with respect to the reference mesh. The results are summarized in the plotting position of the interface at 600 s for the different cases (Fig. 26).

There was an evident impact on the mesh resolution in the zone where the convection was responsible for the

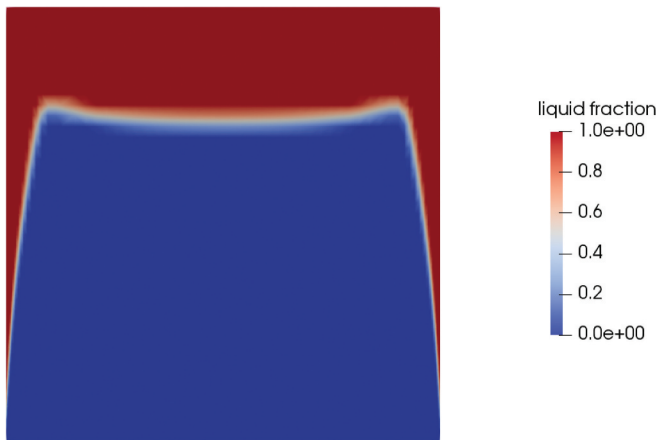


Fig. 23. Interface for the conduction case at 600 s (mid-plane) and variable temperature on the side wall (red is liquid and blue is solid).

wall. In a configuration of the valve in which the opening is determined by the mechanical resistance of the adhesion of the solid plug to the wall, the speed at which the melted layer is formed is crucial to the estimation of the time of opening of the valve.



Fig. 24. Interface for the convection case at 600 s (midplane) and variable temperature on the side wall.

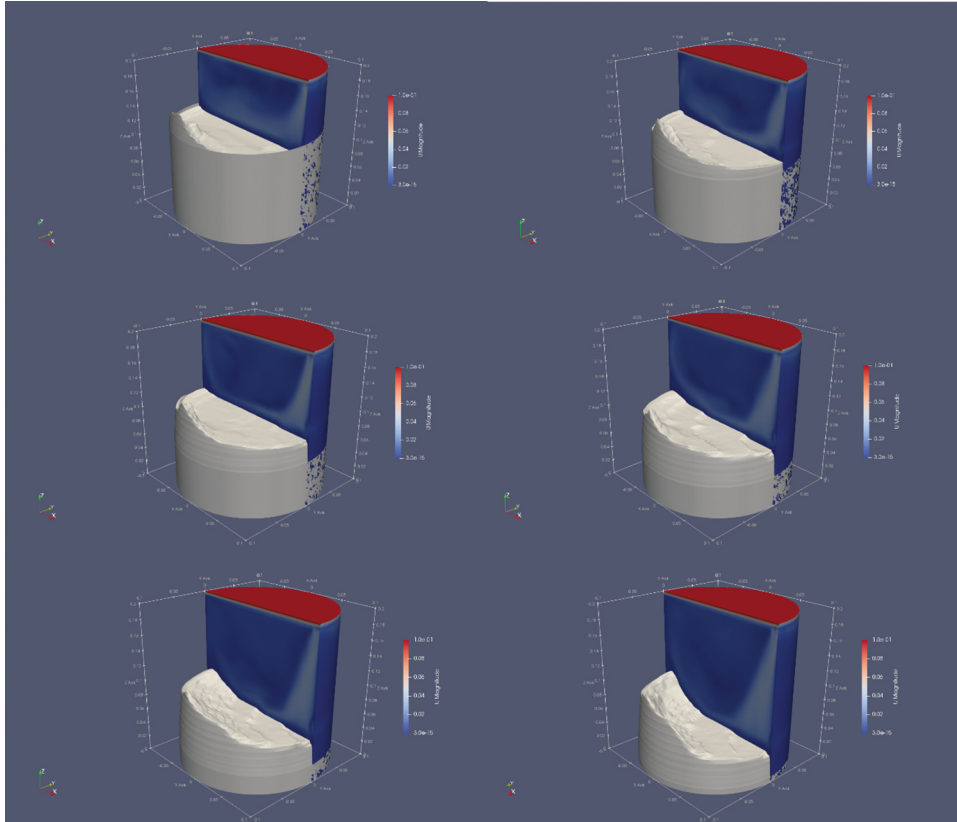


Fig. 25. Shape of the solid plug in time, where deforming is due to the effects of convection. On the right side, the velocity magnitude profile can be seen. The velocity of the upper wall is fixed at 0.1 m/s in the x -direction. On the left side, in white, is the shape of the solid salt. The images shown in this figure are taken at $t = 100$ s (top left), 200 s (top right), 300 s (center left), 400 s (center right), 500 s (bottom left), and 600 s (bottom right).

melting phenomena, i.e., in the center of the cavity where the motion of the fluid promoted the melting. The increased resolution of the eddies given by the use of a finer mesh led to a different evolution of the fluid motion in the cavity that, integrated along the transient, caused a different position at the interface after 600 s. This difference was more evident when comparing the reference mesh and the refined $\times 2$ with respect to the difference between the two refined meshes, indicating an approach toward mesh independence. On the other hand, such differences had a minor impact on the melting time, which was mainly caused by the heat transfer through the wall conduction.

V. CONCLUSION

This paper aims to provide a previously developed OpenFOAM solver with the capability to model solid-liquid phase-change phenomena in light of the safety analysis of the MSFR and the study of freeze plugs as

safety components. The modeling effort was focused on a fixed-grid, temperature-based approach to be compliant with the requirements asked for a reactor-scale representation. To this aim, two well-known algorithms were implemented, namely, the AHC and the ST, along with a novel hybrid method that allows for overcoming some disadvantages in terms of accuracy and computational time. Based on this, a pure conduction and a coupled-conduction-convection solver were developed, the latter being developed with VTM.

The results of the preliminary simulations allowed for drawing some conclusions, both about the developed code and about the freeze valve. For what concerns the developed code, after a verification effort, both pure conduction and convection solvers were demonstrated to be suitable for the simulation of a freeze valve. The choice between the two solvers depended on the configuration of the freeze plug system and the kind of transient. For instance, if the safety analysis involved a LOHS accident with the

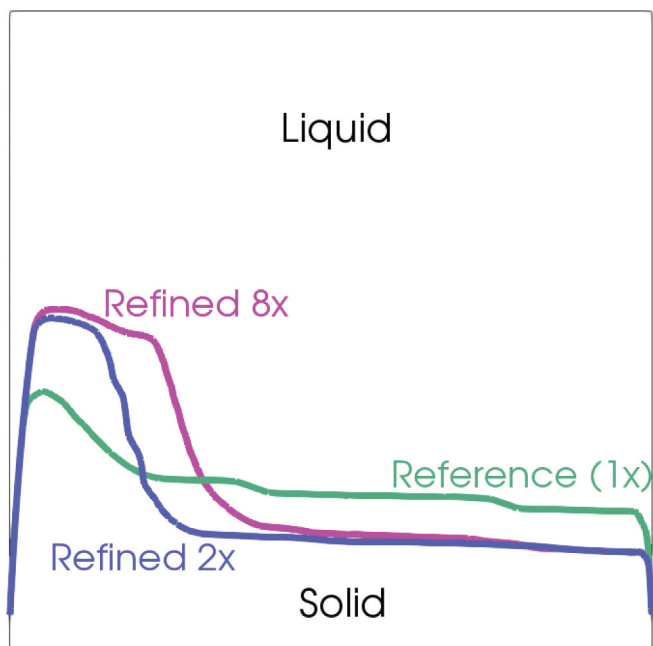


Fig. 26. Shape of the solid-liquid interface at 600 s and at the midplane for the different mesh refinements (in green is the mesh presented in Fig. 16, in blue is the 2 \times refinement, and in purple is the 8 \times refinement).

forced convection of the liquid salt in the primary system, the use of a convective solver was preferable, especially if the valve was located close to the primary circuit. On the other hand, if the movement of the liquid was negligible, the conduction solver could help reduce the computational effort.

As for the design of the freeze valve, the outcomes underline that the freeze valve cannot act as a passive safety system in conditions of adiabatic walls since the time to melt the valve during a transient is well beyond acceptable limits, especially in pure conduction, but also considering the convective contribution. This calls for a solution that involves the melting of the freeze plug not from the top of the system but from the sides, as proposed by other works.^[4,10,15]

In terms of future development, given the relevance of the structural components surrounding the freeze plug, the development of a multiregion solver capable of dealing with the different components (valve, metal walls, etc.) of the freeze plug system is of remarkable importance. In terms of boundary conditions, the influence of the primary circuit should be carefully considered, both during nominal operations and during accident scenarios. Even if in this work reasonable boundary conditions were selected, the evolution of the accident transient should be considered directly, implementing the algorithm proposed inside a multiphysics reactor-scale simulation tool. In this

way, it will be possible to have a tool that can help in the design and optimization of the freeze plug both in terms of location and performance.

Acronyms

- 1-D = one-dimensional
- 2-D = two-dimensional
- AHC = Apparent Heat Capacity Method
- CMT = Continuum Mixture Theory
- DST = Darcy Source Term
- LHM = Latent Heat Modeling
- LOHS = loss of heat sink
- MSFR = molten salt fast reactor
- MSR = molten salt reactor
- MSRE = Molten Salt Reactor Experiment
- PCM = phase-change materials
- ST = Source Term method
- VTM = Velocity Transition Modeling

Nomenclature

- a_{nb} = coefficient of the neighbors of the control volume “ p ” in the discretized energy equation
- a_p = coefficient of the control volume “ p ” in the discretized energy equation
- b = coefficient of the source term in the discretized energy equation
- C = Darcy source term’s constant
- c_p = weighted average of the solid and liquid specific heat capacities
- $c_{p,l}$ = specific heat capacity of the liquid
- $c_{p,s}$ = specific heat capacity of the solid
- dT = temperature difference between the solidus and the liquidus
- \vec{F} = momentum exchange source term
- f = liquid mass fraction
- g = liquid volume fraction
- \vec{g} = gravity acceleration

H = volumetric enthalpy of the mixture

H_p = average volumetric enthalpy over the control volume “ p ”

h = specific enthalpy of the mixture

h_l = specific enthalpy of the liquid

h_0 = specific enthalpy of the solid at the melting temperature T_m

h_s = specific enthalpy of the solid

k = thermal conductivity

L = latent heat

\vec{n} = normal to the solid-liquid interface

\bar{p} = liquid’s kinematic pressure

Q = energy source term

\vec{q} = heat flux

S_p = linearization coefficient for H_p (diagonal term)

S_u = linearization coefficient for H_p (source term)

T = temperature

T_m = melting temperature

\vec{u} = velocity field, velocity

v = velocity of the solid-liquid interface

Greek

ϵ = half of dT

ρ = weighted average of the solid and liquid densities

ρ_l = density of the liquid

ρ_s = density of the solid

$\widehat{\rho c_p}$ = weighted average heat capacity

ν_l = kinematic viscosity of the liquid

Disclosure Statement

No potential conflict of interest was reported by the authors.

Funding

This project received funding from the Euratom research and training programme 2014–2018 under grant agreement no. 847527.

Research Data

The data that support the findings of this study are openly available in Zenodo at this address: <http://doi.org/10.5281/zenodo.755514>.

Disclaimer

The content of this paper does not reflect the official opinion of the European Union. Responsibility for the information and/or views expressed therein lies entirely with the authors.

ORCID

Stefano Lorenzi  <http://orcid.org/0000-0003-2747-1825>

References

1. “Generation IV International Forum 2016 Annual Report,” Generation IV International Forum (2016).
2. D. GERARDIN et al., “Design Evolutions of Molten Salt Fast Reactor,” presented at the Int. Conf. on Fast Reactors and Related Fuel Cycles: Next Generation Nuclear Systems for Sustainable Development, June 26. Yekaterinburg, Russia (2017).
3. B. M. CHISHOLM, S. L. KRAHN, and A. G. SOWDER, “A Unique Molten Salt Reactor Feature—The Freeze Valve System: Design, Operating Experience, and Reliability,” *Nucl. Eng. Des.*, **368**, 110803 (2020); <https://doi.org/10.1016/j.nucengdes.2020.110803>.
4. M. TIBERGA et al., “Preliminary Investigation on the Melting Behavior of a Freeze-Valve for the Molten Salt Fast Reactor,” *Ann. Nucl. Energy*, **132**, 544 (2019); <https://doi.org/10.1016/j.anucene.2019.06.039>.
5. V. VOULGARPOULOS et al., “Transient Freezing of Water Between Two Parallel Plates: A Combined Experimental and Modelling Study,” *Int. J. Heat Mass Trans.*, **153**, 119596 (2020); <https://doi.org/10.1016/j.ijheatmasstransfer.2020.119596>.
6. G. CARTLAND GLOVER, “On the Numerical Modelling of Frozen Walls in a Molten Salt Fast Reactor,” *Nucl. Eng. Des.*, **365**, 110290 (2019); <https://doi.org/10.1016/j.nucengdes.2019.110290>.
7. S. C. GUPTA, *The Classical Stefan Problem: Basic Concepts, Modelling, and Analysis*, No. V. 45 in North-Holland Series in Applied Mathematics and Mechanics, Elsevier (2003).

8. V. ALEXIADES and A. D. SOLOMON, *Mathematical Modelling of Melting and Freezing Processes*, Hemisphere Publishing Corporation (1993).
9. A. ONUKI, *Phase Transition Dynamics*, Cambridge University Press (2002).
10. M. TANO RETAMALES, “Development of Multi-Physical Multi-Scale Models for Molten Salts at High Temperature and Their Experimental Validation,” PhD Thesis, University of Grenoble Alpes, LPSC - Laboratoire de Physique Subatomique et de Cosmologie (2018).
11. J. H. NAZZI EHMS et al., “Fixed Grid Numerical Models for Solidification and Melting of Phase Change Materials (PCMs),” *Appl. Sci.*, **9**, 20, 4334 (2019); <https://doi.org/10.3390/app9204334>.
12. C. R. SWAMINATHAN and V. R. VOLLER, “A General Enthalpy Method for Modeling Solidification Processes,” *Metall. Trans. B*, **23**, 5, 651 (1992); <https://doi.org/10.1007/BF02649725>.
13. Q. LI et al., “Preliminary Study of the Use of Freeze-Valves for a Passive Shutdown System in Molten Salt Reactors,” presented at the ASME/NRC 2014 12th Valves, Pumps, and Inservice Testing Symp., Rockville, Maryland, American Society of Mechanical Engineers (2014).
14. I. K. AJI et al., “An Experimental Study on Freeze Valve Performance in a Molten Salt,” Volume 9: Student Paper Competition, American Society of Mechanical Engineers, London, England (2018).
15. V. GIRAUD et al., “Development of a Cold Plug Valve with Fluoride Salt,” *EPJ Nucl. Sci. Technol.*, **5**, 9, 9 (2019); <https://doi.org/10.1051/epjn/2019005>.
16. E. CERVI et al., “Development of a Multiphysics Model for the Study of Fuel Compressibility Effects in the Molten Salt Fast Reactor,” *Chem. Eng. Sci.*, **193**, 379 (2018); <https://doi.org/10.1016/j.ces.2018.09.025>.
17. E. CERVI et al., “Multiphysics Analysis of the MSFR Helium Bubbling System: A Comparison Between Neutron Diffusion, SP3 Neutron Transport and Monte Carlo Approaches,” *Ann. Nucl. Energy*, **132**, 227 (2019); <https://doi.org/10.1016/j.anucene.2019.04.029>.
18. E. CERVI et al., “Development of an SP₃ Neutron Transport Solver for the Analysis of the Molten Salt Fast Reactor,” *Nucl. Eng. Des.*, **346**, 209 (2019); <https://doi.org/10.1016/j.nucengdes.2019.03.001>.
19. F. CARUGGI et al., “Multiphysics Modelling of Gaseous Fission Products in the Molten Salt Fast Reactor,” *Nucl. Eng. Des.*, **392**, 111762 (2022); <https://doi.org/10.1016/j.nucengdes.2022.111762>.
20. C. BONACINA et al., “Numerical Solution of Phase-Change Problems,” *Int. J. Heat Mass Trans.*, **16**, 10, 1825 (1973); [https://doi.org/10.1016/0017-9310\(73\)90202-0](https://doi.org/10.1016/0017-9310(73)90202-0).
21. A. D. BRENT, V. R. ROLLER, and K. J. REID, “Enthalpy-Porosity Technique for Modelling Convection-Diffusion Phase Change: Application to the Melting of a Pure Metal,” *Numer. Heat Transfer*, **13**, 3, 297 (1988); <https://doi.org/10.1080/10407788808913615>.
22. W. BENNON and F. INCROPERA, “A Continuum Model for Momentum, Heat and Species Transport in Binary Solid-Liquid Phase Change Systems—I. and II,” *Int. J. Heat Mass Trans.*, **30**, 10, 2161 (1987); [https://doi.org/10.1016/0017-9310\(87\)90094-9](https://doi.org/10.1016/0017-9310(87)90094-9).
23. R. VISWANATH and Y. JALURIA, “A Comparison of Different Solution Methodologies for Melting and Solidification Problems in Enclosures,” *Numer. Heat Transfer Part B*, **24**, 1, 77 (1993); <https://doi.org/10.1080/10407799308955883>.
24. V. R. VOLLER and C. R. SWAMINATHAN, “General Source-Based Method for Solidification Phase Change,” *Numer. Heat Transfer Part B*, **19**, 2, 175 (1991); <https://doi.org/10.1080/10407799108944962>.
25. N. HANNOUN, V. ALEXIADES, and T. Z. MAI, “A Reference Solution for Phase Change with Convection,” *Int. J. Numer. Method*, **48**, 11, 1283 (2005); <https://doi.org/10.1002/fld.979>.
26. M. TORABI RAD, *Solidification Melting Source: A Built-in fvOption in OpenFOAM® for Simulating Isothermal Solidification*, Springer International Publishing (2019); https://doi.org/10.1007/978-3-319-60846-4_32.
27. J. STEFAN, “Über einige Probleme der Theorie der Wärmeleitung,” *Sitzungber. Wien, Akad. Mat. Natur*, **98**, 473 (1889).